Supporting Information

Chiral $(BiO)_2CO_3$ Catalysts with Spin-Selective Charge Transport Enhance Photocatalytic Oxygen Evolution

Yuqiang Shi[a§], Zhiwei Sun[a§], Yige Wang[a], Xiaoxiao Fu[a], Zhijia Song[a], Zhaoxiong Xie[a,b] Haixin Lin[a,b]*

[a.]State Key Laboratory of Physical Chemistry of Solid Surfaces, Collaborative Innovation Center of Chemistry for Energy Materials, Department of Chemistry, College of Chemistry and Chemical Engineering, Xiamen University, Xiamen 361005, China.

[b.]Innovation Laboratory for Sciences and Technologies of Energy Materials of Fujian Province (IKKEM), Xiamen 361005, China.

§ Y. S. and Z. S. contributed equally to this work.

Corresponding authors: Haixin Lin * Email: haixinlin@xmu.edu.cn

Experimental Section

1. Materials.

Urea (CH_4N_2O, ≥99.5%), sodium carbonate (Na_2CO_3, ≥99.5%), D-sucrose ($C_{12}H_{22}O_{11}$, 98%), bismuth nitrate ($Bi(NO_3)_3$, 98%), sodium hydroxide (NaOH, 98%), potassium hydroxide (KOH, 97%), nitric acid (HNO_3, 65%~68%), silver nitrate ($AgNO_3$, 99%), potassium iodide (KI, 97%), potassium hydrogen phthalate ($C_8H_5KO_4$, 98%), sodium sulfite (Na_2SO_3, 98%), hydrogen peroxide (H_2O_2, 30%), and absolute ethanol (C_2H_5OH, 99%) were all purchased from Sinopharm Chemical Reagent Co., Ltd.; 5,5-dimethyl-1-pyrroline N-oxide (DMPO) was purchased from Sigma-Aldrich; Ar (99.999%) was purchased from Linde Gas Co., Ltd.; ultrapure water (resistivity ≥18.2 MΩ·cm) was prepared using a CREATE FUN laboratory ultrapure water system. All chemicals were used without further purification.

2. Preparation of the catalysts

2.1 Synthesis of BOC-U samples with different chirality

BOC-U samples with different chirality were synthesized via a hydrothermal method. Specifically, nitric acid (4 mol/L, 5 mL), sodium hydroxide solution (2 mol/L, 11.75 mL), bismuth nitrate (1.16 mmol), and sucrose (0.73 mmol, 0.876 mmol, or 1.169 mmol) were sequentially added into a Teflon liner and stirred for 30 minutes to ensure homogeneity. This corresponded to sucrose-to-bismuth (Sucrose/Bi) molar ratios of 0.63, 0.76, and 1.01, respectively. The mixture was then transferred to an autoclave and heated in an oven at 453 K for 6 hours. Subsequently, the resulting product was collected by centrifugation and washed twice with ultrapure water to remove residual reactants. The samples obtained at Sucrose/Bi ratios of 0.76, 0.63, and 1.01 were denoted as BOC-SC-U, BOC-MC-U, and BOC-WC-U, respectively.

2.2 Preparation of BOC samples with different chirality

BOC-U sample (100 mg) was dispersed in 10 mL of water. Subsequently, 5 mL of hydrogen peroxide solution was added, and the mixture was stirred overnight. After the reaction, the product was collected by centrifugation and washed four times with ultrapure water to remove residual reactants. The resulting materials, obtained by treating the BOC-U

samples synthesized with different amounts of sucrose, were designated as BOC-SC, BOC-MC, and BOC-WC, respectively.

2.3 Role of sucrose as a chiral-directing agent

In this work, sucrose plays dual roles under hydrothermal conditions, functioning both as a chiral-directing agent and as an in situ carbon source for carbonate formation. The chemical and structural functions of sucrose during the synthesis process can be understood from two interconnected aspects.

Under alkaline hydrothermal conditions, sucrose first undergoes hydrolysis into monosaccharides, followed by dehydration, rearrangement, and fragmentation reactions, generating oxygenated intermediates and small organic molecules. These species are further oxidized into CO_2 or inorganic carbon-containing species in the presence of oxidizing environments within the reaction system. The generated CO_2 subsequently reacts with OH^- to form HCO_3^-/CO_3^{2-}, which combines with Bi^{3+} ions to produce $(BiO)_2CO_3$ through an in-situ mineralization process. Compared with direct addition of carbonate salts, this gradual release of carbonate species enables controlled nucleation and crystal growth. [1-4]

Meanwhile, owing to its multiple vicinal hydroxyl groups and intrinsic stereochemical configuration, sucrose can adsorb selectively on crystal growth interfaces through hydrogen bonding and coordination interactions. Such interfacial interactions locally break growth symmetry and induce anisotropic crystal growth, allowing molecular chirality to be transferred from organic species to the inorganic framework. The continuous supply of carbonate species further stabilizes the interfacial organization of sucrose molecules, facilitating progressive amplification of chiral information from molecular interactions to mesoscale chiral morphologies.

3. Characterizations of the catalysts

The Bruker D8 Advance diffractometer, operated at 40 kV and 30 mA with a Cu-Kα radiation source, was used for X-ray diffraction analysis. Transmission electron microscopy images were collected on a Tecnai F30 instrument equipped with a STEM unit and an HAADF detector, operating at an acceleration voltage of 300 kV. Circular dichroism spectra of the samples were measured with a JASCO J-1700 spectrometer. Surface chemical compositions

was analyzed by X-ray photoelectron spectroscopy (XPS, Escalab Xi+, Thermo Fisher). UV-vis diffuse reflectance spectra (UV-vis DRS) were recorded on a UV-vis spectrophotometer (Cary 5000, Agilent), with $BaSO_4$ as reference. Steady state photoluminescence (PL) was recorded utilizing the F-7000 (Hitachi). The model of water contact angle measuring instrument is OCA20, manufactured by the German company Dataphysics. Fourier transform infrared (FT-IR) spectra were recorded on an IR spectrometer (Nicolet iS50, Thermo Scientific). Electron spin resonance (ESR) spectra were obtained on an ESR spectrometer (Bruker, EMX-10/12). Scanning electron microscope images were obtained using field-emission scanning electron microscopes, Hitachi SU8600 and Hitachi S-4800. Extinction measurements were performed using a UV-vis spectrophotometer (PerkinElmer, LAMBDA 1050+). The specific surface areas were determined by conducting N_2 adsorption–desorption analysis on a Micromeritics (ASAP2460) surface area analyzer, employing the Brunauer–Emmett–Teller (BET) method. Some measured circular dichroism spectra were smoothed.

4. Magnetic conductive-probe atomic force microscopy (mc-AFM) measurement.

The primary objective is to evaluate the electrical properties of the samples by measuring the I–V curves and calculating the spin polarization (*P*) of the samples. Prior to testing, the sample was uniformly coated onto an FTO glass substrate, which was then electrically connected to the AFM base using conductive adhesive. The conductive probe was pre-magnetized upward (or downward) for 3–5 minutes using a permanent magnet. I–V curves were recorded within a voltage range of -10 V to 10 V at a frequency of 0.5 Hz. A bias voltage was applied to the sample, and measurements were repeated more than 50 times to ensure reliability, with the results averaged. Based on the measured I–V differences, the spin polarization (*P*) can be quantified using the following equation:

$$P = \frac{I_{up} - I_{down}}{I_{up} + I_{down}} * 100\%$$

where I_{up} and I_{down} represent the currents measured when the tip is magnetized in the upward or downward direction, respectively.

5. Photoelectrochemical measurements

The photoelectrochemical testing system mainly consists of four parts: an electrochemical workstation, an H-type electrolytic cell, a xenon lamp light source (Beijing Perfect Light Technology Company, PLS-SXE300), and a circulating cooling device. This system can be used to characterize the Mott-Schottky curve, transient photocurrent response (i-t), electrochemical impedance spectroscopy (EIS), open-circuit potential (OCP), and linear scanning voltammetry (LSV) of photocatalysts. These measurements allow for the investigation of various photoelectric properties of the photocatalyst, including its band structure, charge separation efficiency, and charge transfer resistance. During photoelectrochemical testing, an aqueous solution of 0.1 mol L^{-1} Na_2SO_4 is used as the electrolyte. A three-electrode system is employed, consisting of a working electrode made of conductive glass uniformly coated with a photocatalyst film, a Pt mesh counter electrode, and an Ag/AgCl reference electrode. To maintain temperature stability during light exposure, the temperature is controlled at 20 °C using a circulating cooling device.

Preparation of the working electrode: 3 mg of the photocatalyst is added to 1 mL of isopropanol and dispersed uniformly by ultrasonication. Subsequently, 20 μL of Nafion solution is added, and the mixture is further ultrasonicated for 1 hour to obtain a uniformly dispersed suspension. Next, 100 μL of the suspension is evenly drop-cast onto a piece of conductive glass (1 × 3 cm^2) using a pipette and allowed to dry naturally at room temperature.

6. Photocatalytic oxygen evolution

Photocatalytic water oxidation tests were conducted using a LABSOLAR water splitting system (Beijing Perfectlight Technology Co., Ltd.). Oxygen production was measured by connecting a gas chromatograph (Tianmei GC7900) to the photocatalytic reaction system. First, 30 mg of the catalyst was dispersed in 100 mL of water, and 170 mg of $AgNO_3$ was added as a sacrificial agent. The reaction solution was then transferred into the reactor. Subsequently, the reactor was connected to the reaction setup, and the system was evacuated using a vacuum pump. A xenon lamp (300 W, with an irradiation intensity of ~770 mW/cm^2) was vertically positioned above the reactor for illumination. The reaction proceeded for 3 hours under continuous stirring and light exposure. The photocatalytic setup was programmed to automatically inject gas samples into the gas chromatograph at regular intervals. The produced

gases were detected using a gas chromatograph (SHIMADXU GC-2014C) equipped with a flame ionization detector (FID) and a thermal conductivity detector (TCD).

7. H_2O_2 detection

The photoelectrochemical reaction was performed in 0.1 M Na_2SO_4 solution at a constant potential of 1.23 V vs. RHE for 3 h. The hydrogen peroxide (H_2O_2) concentration was then determined using the iodometric method. Specifically, 0.25 mL of the reaction solution was mixed with 1.75 mL of deionized water, 1 mL of 0.4 mol/L potassium iodide (KI) solution, and 1 mL of 0.1 mol/L potassium hydrogen phthalate ($C_8H_5KO_4$) solution. The mixture was allowed to stand for 30 min. Under acidic conditions, hydrogen peroxide (H_2O_2) reacts with iodide ions (I^-) to form triiodide ions (I_3^-) (reaction: $H_2O_2 + 3I^- + 2H^+ \rightarrow I_3^- + 2H_2O$), which exhibits a strong absorption peak at around 350 nm. The absorbance at 350 nm was measured by UV-vis spectroscopy to calculate the total amount of hydrogen peroxide produced during the reaction.

8. Rhodamine B Degradation

30 mg of the BOC catalyst was added to 100 mL of a Rhodamine B solution with a concentration of 200 μmol/L to prepare the reaction solution. The mixture was then magnetically stirred in the dark for 30 minutes to achieve adsorption-desorption equilibrium, while the temperature was maintained at a constant 25°C throughout the experiment. A xenon lamp (300 W, with an irradiation intensity of ~770 mW/cm^2) was vertically positioned above the reactor for illumination. During the reaction, samples of the solution were collected at 20-minute intervals, immediately centrifuged, and analyzed using a UV-vis spectrophotometer to evaluate the photocatalytic activity.

9. g-factor calculation

g-factor = CD/ (32980*abs.)

10. The calculation method of the internal electric field (IEF) magnitude

The internal electric field (IEF) magnitude was calculated by the equation developed by Kanata et al.: $F_S = (-2\rho V_S/\varepsilon\varepsilon_0)^{1/2}$, in which F_s is the IEF magnitude, ρ is the surface charge density, V_S is the surface voltage, ε is the low-frequency dielectric constant, and ε_0 is the

permittivity of free space (ε and ε_0 are two constants). It can be found that the IEF magnitude is mainly determined by V_s and ρ. To assess their IEF magnitude, V_s was surveyed via open-circuit potential measurements, and ρ was determined through the transient photocurrent density measurements. Integrating the measured transient photocurrent density minus the steady-state values of photocurrent with respect to time yields a value that is proportional to the number of negative charges accumulated at the surface. As depicted in Figure 6b, the calculated integral areas for BOC-SC, BOC-MC, and BOC-WC were 3.067, 2.826, and 1.391, respectively. In other words, their surface charge densities were 3.067, 2.826, and 1.391 μC/cm^2, respectively. As depicted in Figure 6a, the OCP for BOC-SC, BOC-MC, and BOC-WC were 570 mV, 480mV, and 450 mV, respectively. Under the assumption that the intensity of BOC-WC was normalized to "1", the IEF magnitude were calculated to be 1.67, 1.43, and 1 for BOC-SC, BOC-MC, and BOC-WC, respectively, using the aforementioned equation.

Supplementary results

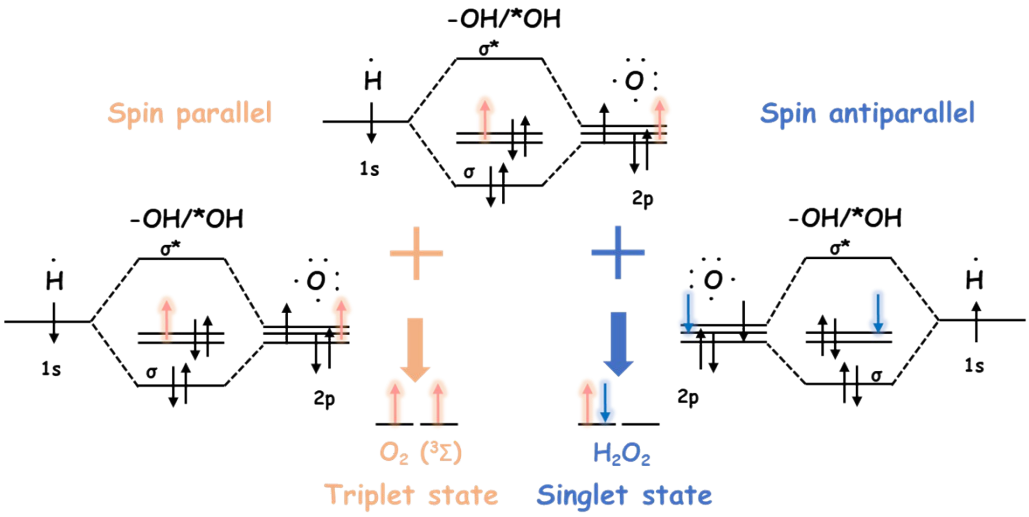

Figure S1 ·OH radicals with different initial spin orientations give rise to singlet or triplet products.

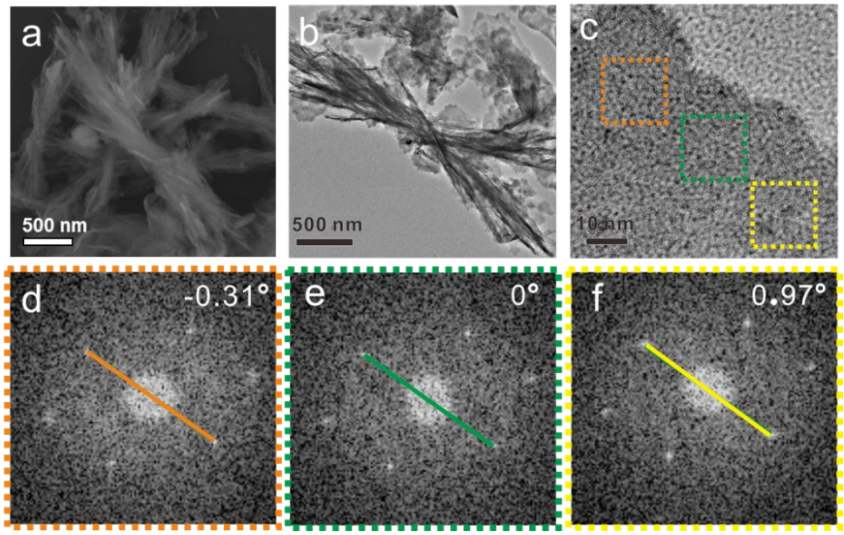

Figure S2 Chiral structure characterization of BOC-SC-U. (a) Low magnification SEM image. (b) Low magnification TEM image. (c) High magnification TEM image of sheet. (d-f) FFT of sheet showing lattice distortion.

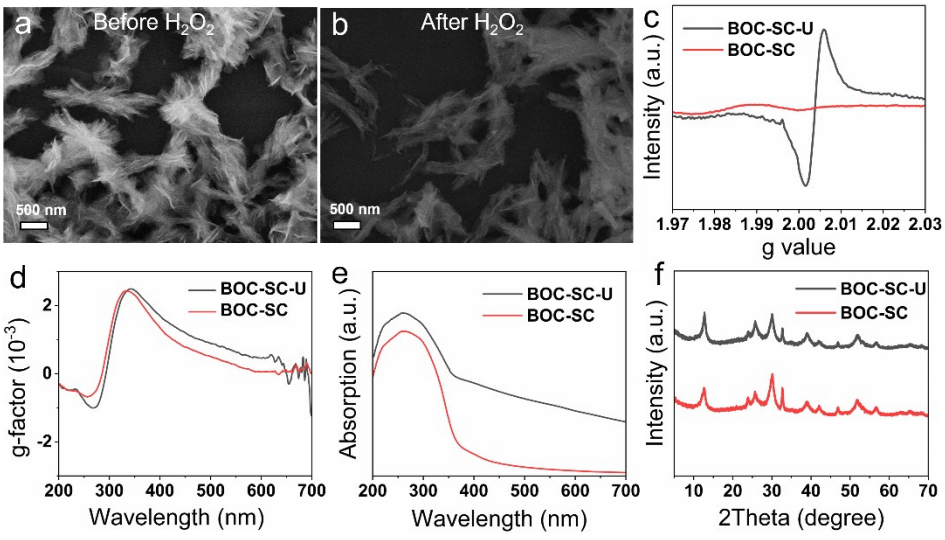

Figure S3 Comparison of strongly chiral BOC before and after hydrogen peroxide treatment. (a) SEM image before H_2O_2 treatment. (b) SEM image after H_2O_2 treatment. (c) ESR spectra. (d) g-factor. (e) UV-vis DRS. (f) XRD patterns.

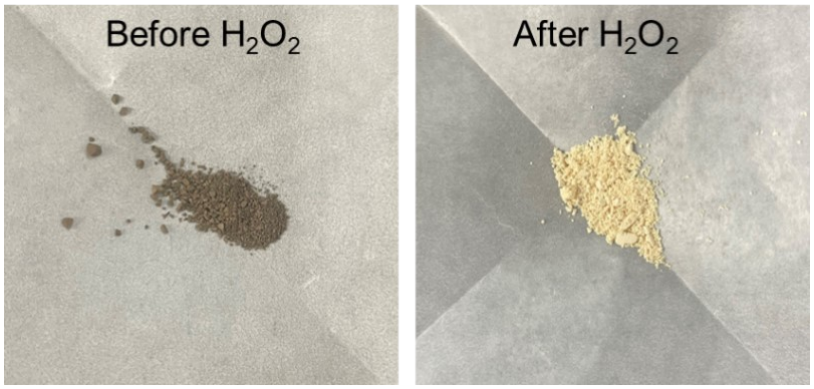

Figure S4 Macroscopic color of strongly chiral BOC before and after hydrogen peroxide treatment.

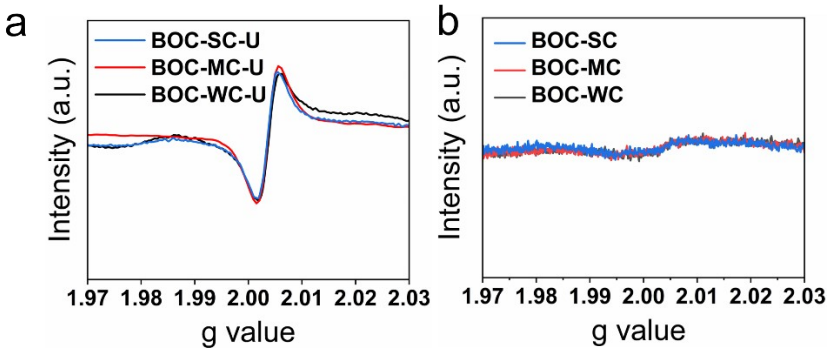

Figure S5 Samples with different chirality before and after hydrogen peroxide treatment. (a) before, (b) after.

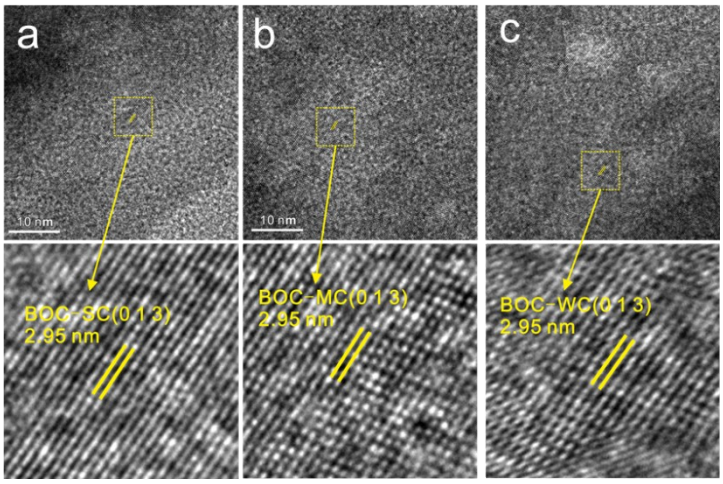

Figure S6 High-resolution TEM images and lattice spacings of the samples with different chirality. (a) BOC-SC. (b) BOC-MC. (c) BOC-WC.

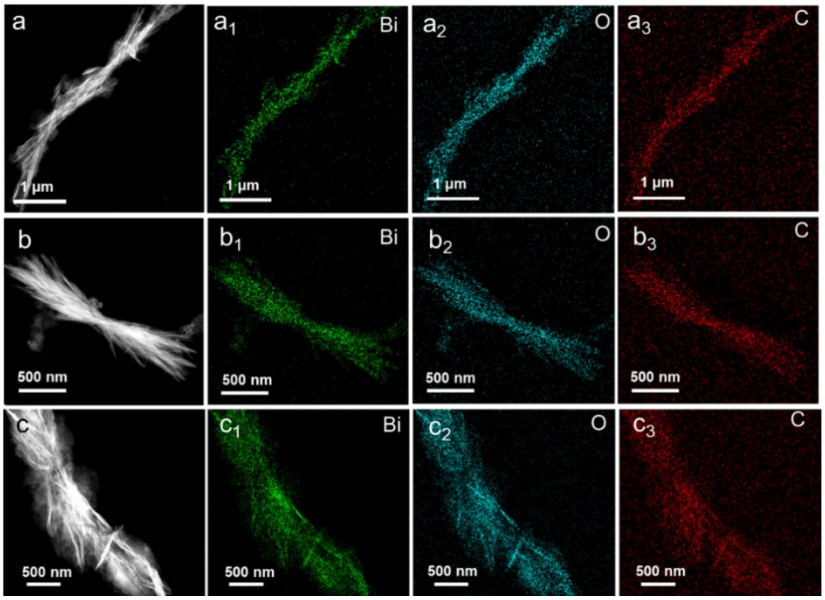

Figure S7 Elemental mapping images of the samples with different chirality. (a) BOC-SC, (b) BOC-MC, (c) BOC-WC.

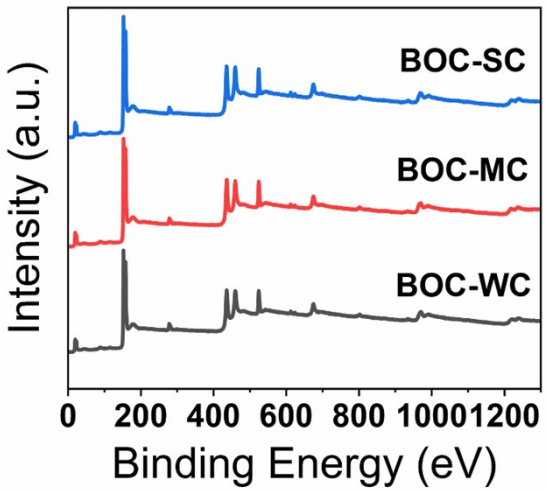

Figure S8 XPS spectra of the samples with different chirality.

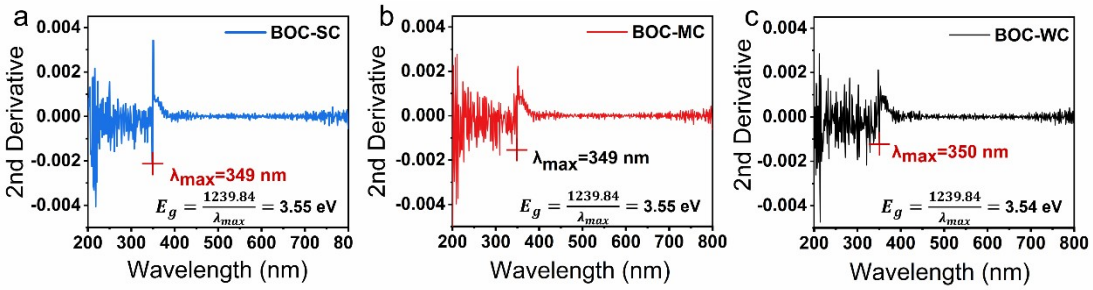

Figure S9 Second-order derivative results of the UV-vis absorption. (a) BOC-SC, (b) BOC-MC, and (c) BOC-WC. The calculated band gaps (E_g) for BOC-SC, BOC-MC, and BOC-WC are 3.55 eV, 3.55 eV, 3.54 eV.

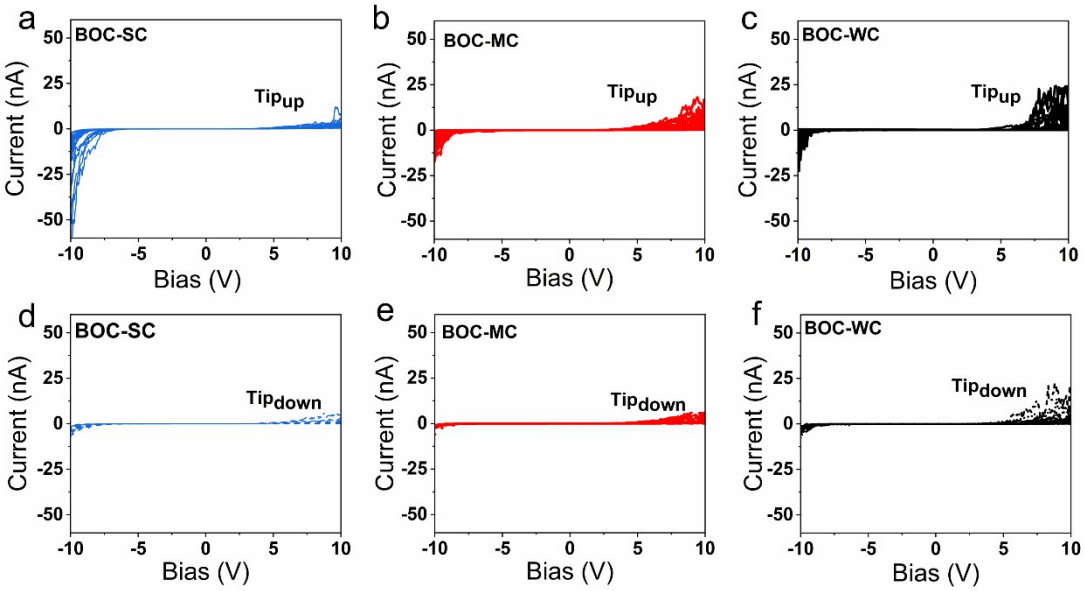

Figure S10 Raw data of I-V curves measured by mc-AFM at different sample positions for the samples with different chirality. (a)-(c) With the tip magnetized upward. (d)-(f) With the tip magnetized downward.

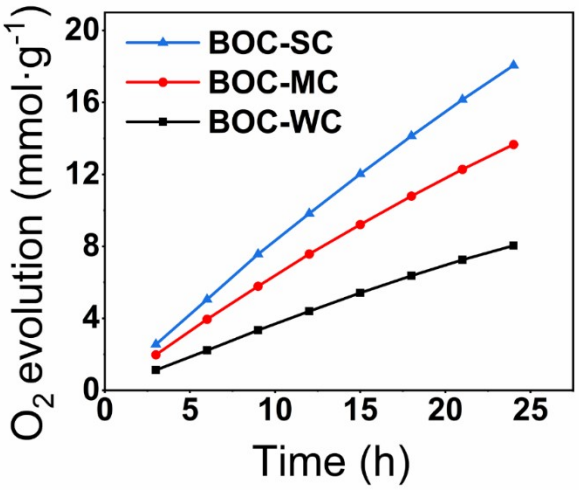

Figure S11 Long-term stability test of the samples with different chirality.

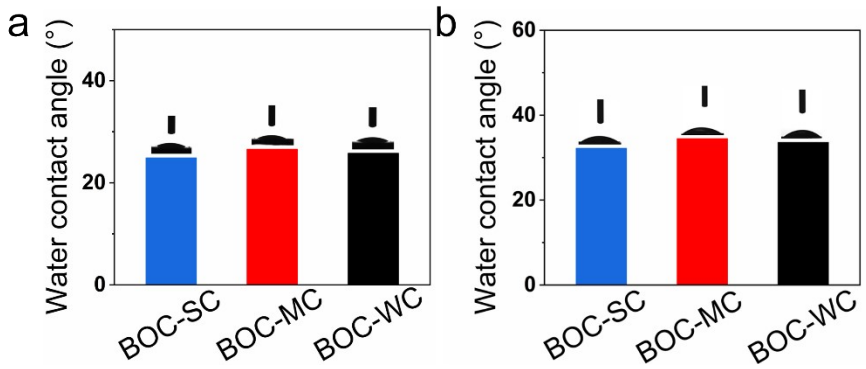

Figure S12 Water contact angle tests on the surface. (a) before photocatalytic oxygen evolution and (b) after photocatalytic oxygen evolution.

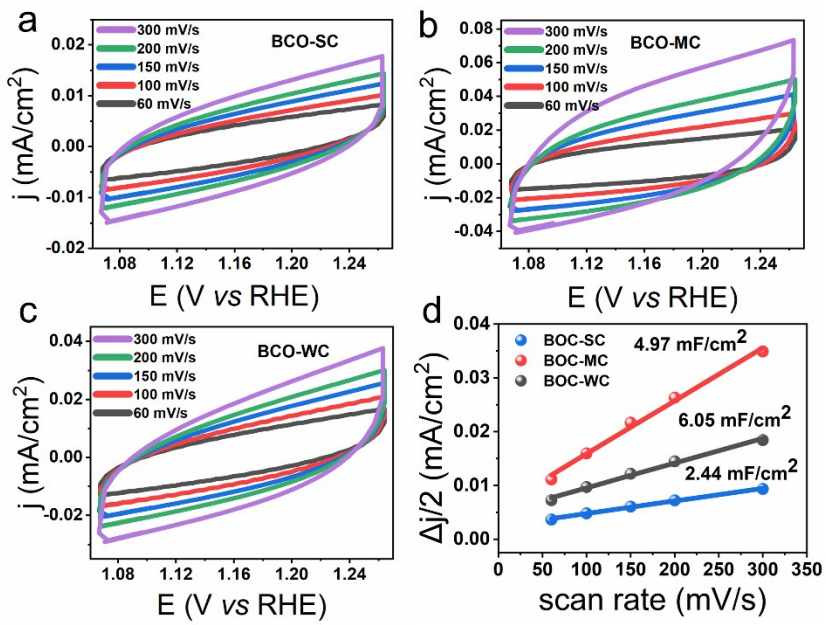

Figure S13 Determination of double-layer capacitance (C_{dl}) for evaluating electrochemical active surface area (ECSA). Cyclic voltammetry (CV) curves measured within a non-Faradaic potential window at scan rates of 50–300 mV s^{-1} for (a) BOC-SC, (b) BOC-MC, and (c) BOC-WC in 0.1 M KOH using an Ag/AgCl reference electrode. (d) Linear plots of capacitive current density difference ($\Delta j = (j_a - j_c)/2$) as a function of scan rate. The slopes correspond to C_{dl} values, which were used for subsequent ECSA estimation.

The electrochemical active surface area (ECSA) of the samples was estimated from the electrochemical double-layer capacitance (C_{dl}) obtained by cyclic voltammetry (CV) measurements. All measurements were carried out in 0.1 M KOH electrolyte using an Ag/AgCl reference electrode and a Pt foil counter electrode. To avoid contributions from Faradaic reactions or photoinduced processes, the

measurements were performed under dark conditions within a non-Faradaic potential window.CV curves were recorded at scan rates of 60, 100, 150, 200, and 300 mV s^{-1}. At each scan rate, the anodic (j_a) and cathodic (j_c) current densities at the selected potential were extracted, and the capacitive current density was calculated using $\Delta j = (j_a - j_c)/2$. The C_{dl} was determined from the slope of the linear fitting between Δj and the scan rate (v), assuming a linear relationship between capacitive current and scan rate. The obtained C_{dl} values were 6.05, 4.97, and 2.44 mF cm^{-2} for BOC-WC, BOC-MC, and BOC-SC, respectively. The ECSA was estimated according to the relationship:

$$\mathrm{ECSA} = C_{dl} / C_s$$

where C_s represents the specific capacitance of a smooth surface.

A commonly adopted literature value of $C_s = 40$ μF cm^{-2} (0.040 mF cm^{-2}) was used for estimation. Based on this assumption, the calculated ECSAs (expressed as cm^2 per geometric cm^2) were 151.25 for BOC-WC, 124.25 for BOC-MC, and 61.00 for BOC-SC. It should be noted that the absolute ECSA values depend on the choice of C_s; therefore, the calculated values are mainly used for relative comparison among samples rather than absolute surface quantification. To evaluate the intrinsic catalytic activity per active site, the current density was further normalized by ECSA using:

$$j_{ECSA} = j_{geo} / \mathrm{ECSA}$$

where j_{geo} is the geometric current density measured at 1.23 V vs RHE under illumination.

The measured geometric current densities were 0.0277, 0.0459, and 0.0617 mA cm^{-2} for BOC-WC, BOC-MC, and BOC-SC, respectively. The corresponding ECSA-normalized current densities were calculated to be 1.83×10^{-4}, 3.69×10^{-4}, and 1.01×10^{-3} mA cm^{-2} ECSA for BOC-WC, BOC-MC, and BOC-SC, respectively. Accordingly, the intrinsic unit-area activity of BOC-SC is approximately 2.7 and 5.5 times higher than that of BOC-MC and BOC-WC, respectively.

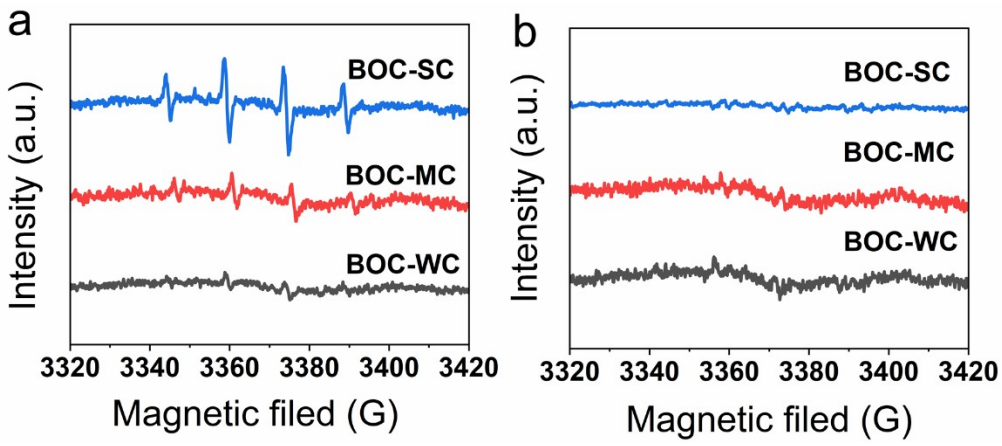

Figure S14 ESR spectra of DMPO-·OH after illumination (a) and before illumination(b).

Table S1 Peak fitting results of XPS O 1s for samples with different chirality.

Simple	Components	Binding Energy (eV)	Percentage(%)
BOC-SC	O-Bi	530.0	29.13
	C-O	531.1	48.54
	[O]	531.9	5.42
	Adsorbed H_2O	532.9	16.91
BOC-MC	O-Bi	530.0	30.28
	C-O	531.1	48.94
	[O]	531.9	5.33
	Adsorbed H_2O	532.9	15.45
BOC-WC	O-Bi	530.0	31.42
	C-O	531.1	49.64
	[O]	531.9	4.23
	Adsorbed H_2O	532.9	14.71

Table S2 EIS fitting parameters.

	R_s (Ω)	R_{ct} (kΩ)	C_d (F)	Wo-R (Ω)	Wo-T(s)	Wo-P
BOC-SC	35.1	22.5	4.95E-5	19.5	5.49E-04	0.471
BOC-MC	32.1	30.6	2.36E-5	3788	1.65	0.754
BOC-WC	30.7	33.4	2.38E-5	3313	1.18	0.761

The equivalent circuit was designed with a serial combination of bulk electrolyte resistance (R_s) and electrochemical interfacial impedance, in which the C_d represents the electrochemical double-layer capacitance, R_{ct} the charge transfer resistance in electrochemical double-layer, W_O the charge transfer resistance induced by diffusion. For BOC-SC, the low-frequency region exhibits a typical 45° line, characteristic of semi-infinite diffusion; the fitted W_O-P is 0.47, close to the theoretical value of 0.5. For BOC-MC and BOC-WC, the depressed low-frequency arcs indicate a transition toward finite diffusion, which is reflected in the higher W_O-P values (0.75–0.76). Consequently, the larger W_O-R and W_O-T for these two samples should be interpreted as a combined effect of diffusion resistance and the deviation from ideal semi-infinite diffusion behavior. Nonetheless, the monotonic trend (BOC-SC < BOC-MC < BOC-WC) is consistent with the performance ranking, confirming that the strongest chirality (BOC-SC) facilitates the fastest ion diffusion. All fitting errors are below 5%, ensuring reliability. The corresponding Nyquist plots with experimental data and fitted curves are provided in Figure 6e.

Reference

1. Q. Li, H. Liu, F. Dong and M. Fu, *J. Colloid Interface Sci.*, 2013, **408**, 33-42.
2. P. Stutzenstein, B. Weiner, R. Köhler, C. Pfeifer and F.-D. Kopinke, *Chem. Eng. J.*, 2018, **339**, 1-6.
3. A. S. Keshari and P. Dubey, *Electrochim. Acta*, 2022, **402**, 139486.
4. S. A. Nicolae, H. Au, P. Modugno, H. Luo, A. E. Szego, M. Qiao, L. Li, W. Yin, H. J. Heeres, N. Berge and M.-M. Titirici, *Green Chem.*, 2020, **22**, 4747-4800.